Institute of Paper Science and Technology
Atlanta, Georgia

IPST TECHNICAL PAPER SERIES

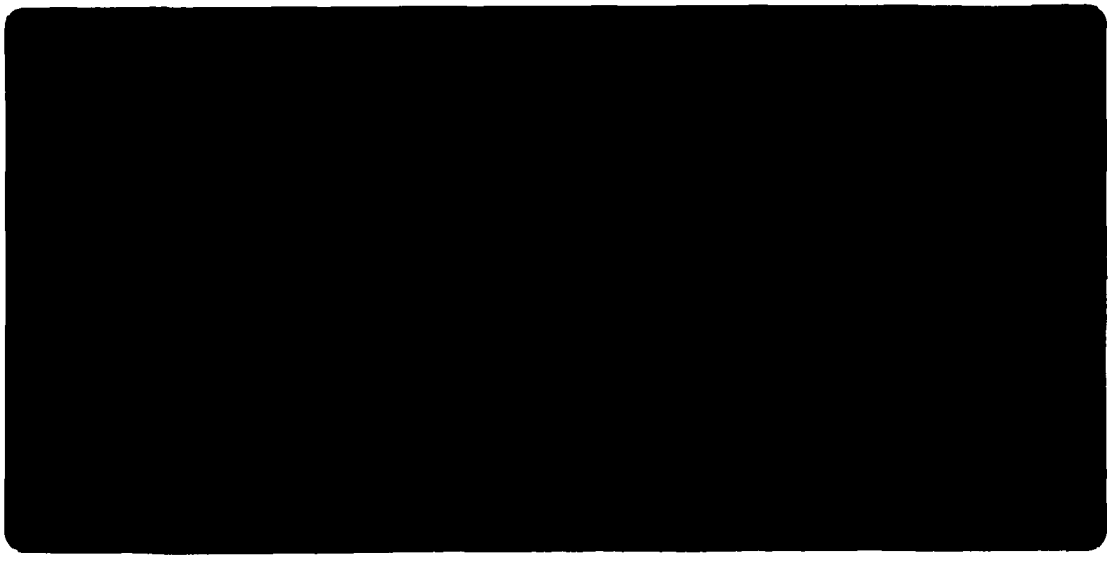

NUMBER 510

RELATIVE FLOW POROSITY IN FIBROUS MEDIA: MEASUREMENTS AND ANALYSIS, INCLUDING DISPERSION EFFECTS

J.D. LINDSAY

JANUARY 1994

Relative Flow Porosity in Fibrous Media: Measurements and Analysis, Including Dispersion Effects

J.D. Lindsay

Submitted to
Tappi Journal

Relative Flow Porosity in Fibrous Media:

Measurements and Analysis, Including Dispersion Effects

Jeffrey D. Lindsay
Associate Professor
Institute of Paper Science and Technology
Atlanta, GA 30318

ABSTRACT

When a fluid flows into the pores of a fibrous material such as paper, the flow behavior will be affected by parameters such as pore size, permeability, surface tension effects, fluid rheology, etc. One key characteristic that has received little attention in the past is the relative flow porosity, defined as the fraction of the total pore space that is open to fluid flow.

When one fluid enters a fibrous mat and displaces another (e.g., air displacing water or wash liquor displacing black liquor), the penetrating fluid only flows through pores that are open to flow. In water-saturated paper, much of the void volume is occupied by water that cannot flow due to chemical or physical absorption and mechanical obstruction (isolated or dead-end pores). In partially saturated paper, surface tension effects may further hinder fluid flow through the sheet. In this paper, we discuss various methods for examining relative flow porosity and present results of new experimental techniques based on in-plane flow measurements.

The experimental approach involves radially injecting known volumes of aqueous, nonabsorbing dye into the center of a compressed, saturated sheet restrained by solid surfaces. The volume of the sheet occupied by the dye is measured, as is the total porosity of the sheet. The ratio of injected dye volume to pore volume within the dyed region is an estimate of effective porosity. This process may be complicated by diffusion and dispersion of the dye flow, but our analytical and numerical analysis of the problem shows these effects can be neglected in some cases.

We show that in unrefined, filler-free paper, effective porosity values are on the order of 40% or more. The relative porosity may be as high as 90% of the extrafiber pore volume. Data for both initially dry and initially saturated sheets are

Term	Definition
Total porosity, ε	Fraction of total volume occupied by pores, or 1 – volume fraction of solid
Effective flow porosity, ε_{eff}	Fraction of total volume occupied by pores open to flow
Relative flow porosity, ε_{rel}	Fraction of the total pore space that is open to flow: $\varepsilon_{rel} = \varepsilon_{eff}/\varepsilon$
Extrafiber porosity, ε_0	Fraction of total volume occupied by pore space between fibers, or 1 – volume fraction of fibers

Table 1. Porosity Definitions.

Relative porosity is especially important when two phases are involved, as when gas displaces liquid, for it governs the speed of the phase boundary. In other words, the penetrating phase can only move through the open, interconnected pores. If the effective porosity of this pore space is small, the penetrating fluid boundary may advance rapidly, yet the amount of penetrating fluid will be small. In two-phase flows, however, capillary effects can cause one phase to obstruct the flow of the other phase, further reducing the effective flow porosity open to each phase.

ESTIMATES OF RELATIVE POROSITY USING PRIOR DATA AND THEORY

In this section, we will find that a variety of concepts in the literature are useful in understanding the distribution of water in a sheet, and can be used to make estimates of relative porosity if we assume that all the pore space outside the swollen cell wall of paper is available to flow. Such logic, however, would imply $\varepsilon_{rel} = 1$ in an unswollen fibrous structure.

A previous study will then be discussed in which a theoretical estimate for relative porosity in an unswollen fibrous web is made. We will modify this result for swollen fibers to obtain a basis for comparing our experimental results reported below.

Extrafiber Pore Space

For paper, the relation between pore space and effective porosity is complicated by the swollen nature of the solid matrix. As a first approximation, one could assume that all the pore space between the swollen fibers in wet paper is available to flow. In other words, ε_o, the extrafiber pore space, might approximate ε_{eff}. In reality, some of the extrafiber pore space will include dead-end pores and possibly other zones of stagnant fluid, so ε_{eff} may be less than ε_o. For now, however, we will neglect the difference.

Water retention ratios.

There are several ways to estimate ε_o. For a computer model of wet pressing, Roux and Vincent (1) estimate it using the water retention ratio (WRR, also called water retention value, WRV) of pulp, reported as grams of water per gram of dry fiber, a measure of the water still held by the fibers after centrifugal dewatering. Effective porosity can then be expressed as:

$$\varepsilon_{eff} \approx \varepsilon_o = \varepsilon - WRR\frac{\rho_s}{\rho_l}(1-\varepsilon), \quad (1)$$

where ρ_s is the dry solid density, generally taken as 1.55 g/cm^3 for cellulose, and ρ_l is the liquid density, 1.0 g/cm^3 for water. Relative porosity is then

$$\varepsilon_{rel} = 1 - WRR\frac{\rho_s}{\rho_l}\left(\frac{1-\varepsilon}{\varepsilon}\right). \quad (2)$$

The difficulty here is that WRR depends on the somewhat arbitrary procedure used, and is not necessarily a valid description of fiber-water interactions in a compressed web. Using a "typical" WRR of 1.7 for a lightly refined chemical pulp, the relationship between total porosity and relative porosity is shown as one of two curves in Figure 1. Once the porosity of a sheet has been reduced below 0.725, Equation 2 yields negative, physically impossible relative porosities. In reality, water will be expressed from the cell wall and from trapped pores as the sheet is compressed, reducing the amount of water retained in the swollen fibers. The experimentally measured WRR is for an essentially uncompressed state. Use of WRR to estimate relative porosity in a paper web is therefore questionable.

Ellis (2) used unusually high g-forces (up to 5×10^4 g, compared to normally used values of 3000 g or less) in a series of WRR measurements to determine the limits on water removal by mechanical forces. Extrapolating his data for several pulps to even higher g-forces, he determined that a WRR value of 0.5 represented the

expected maximum degree of water removal possible by mechanical forces. A WRR of 0.5 represents 33% moisture or 67% solids. A second curve is shown in Figure 2 for a WRR of 0.5. If a water-saturated sheet is compressed to the point where no interfiber pores exist and the WRR is 0.5, then the total porosity at this point is 43.7%, the point at which relative porosity goes to zero. In wet pressing of paper, practical porosity values of the wet sheet are expected to lie between 50 and 80%.

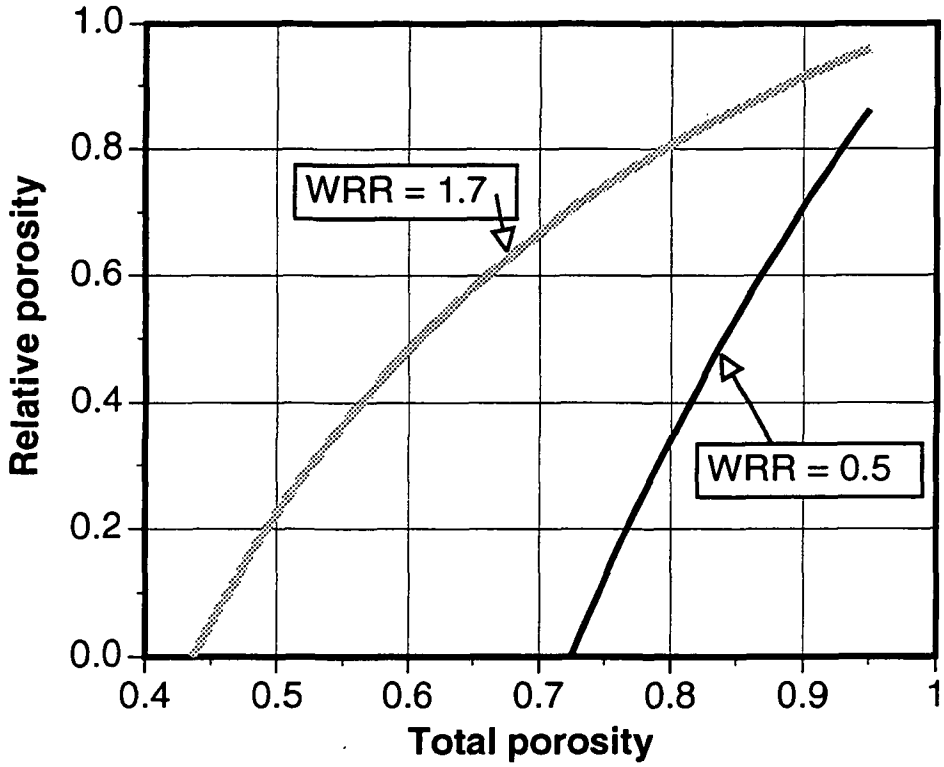

Figure 1. Estimated relative porosities from Equation 2 for two WRR values.

Other measures of associated water.

Several other techniques have been applied to estimate the water held in the cell wall. Robertson (3,4) compares water of association estimates using several techniques (hydrostatic tension, permeability, and dye migration) in uncompressed or lightly compressed webs. Most values were more than 2 gm of water per gm of fiber and may not be useful in describing the pore state of a paper web beyond the forming section of a paper machine.

The solute exclusion technique of Stone and Scallan (5) has also been useful in identifying the amount of water contained in micropores (pores inaccessible to

dextran of a specified molecular weight) in the cell wall. Solute exclusion results are generally consistent with Ellis's high-g WRR results (micropore water content on the order of 30% or greater). Carlsson et al. (6) applied a related method to show that associated water is expressed from micropores as paper is pressed to higher solids levels. One may assume that the water in micropores is trapped and unavailable for flow under an external pressure gradient, but this is not necessarily the case. Some pores may permit throughflow. However, the velocity through such pores will be much smaller for a given pressure gradient than in larger interfiber pores, and their contribution to flow may be negligible.

Kozeny-Carman Analysis

Permeability measurements in paper can be applied to estimate the amount of water immobilized by the swollen fiber. Here permeability is defined as the empirical constant, K, in Darcy's law for unidirectional flow in porous media:

$$v = \frac{K}{\mu}\frac{\Delta P}{L}, \tag{3}$$

where v is the superficial velocity (flow rate divided by area), μ is the fluid viscosity, and ΔP is the pressure drop in the flow direction across a distance L. K, the permeability, has units of length squared.

The permeability of a deformable porous medium changes as it is compressed. Formulas relating permeability and porosity can be derived by making simplifying assumptions about the structure of the medium. For example, by assuming that the pore network consists of many distinct, continuous, and regular channels passing from one end of the porous medium to another, the well-known Kozeny-Carman equation can be obtained:

$$K = \frac{1}{\kappa S_0^2}\frac{\varepsilon_0^3}{(1-\varepsilon_0)^2} \tag{4}$$

where S_0 is the surface area per unit volume of solid material, and κ is a shape factor (the Kozeny constant) that accounts for effects of channel shape and orientation. Note that we have used ε_0 instead of ε (which is usually seen in the Kozeny-Carman equation), for the pore space considered in the derivation is the extrafiber pore space. The water trapped in the cell wall presumably does not contribute to flow and in effect increases the apparent volume of the solid (immobile) phase.

The Kozeny constant, κ, can be derived for ideal, simple pore structures, but becomes an empirical factor for real porous media. In many cases, it is not constant but a function of porosity. For fibrous media, a value of 5.55 is a widely used value which works well in many cases (7), although values typically may lie in the range of 3-7 for porosities less than 0.8 (8). When an empirical factor is used, the effect of dead-end pores and other regions of immobilized fluid on the average velocity or on the permeability is accounted for, but no information about the relative porosity itself can de derived. We will again assume that ε_o approximates ε_{eff}.

The effective volume of the swollen fibers is defined as α, with units of cm^3/g. At a concentration of c g/cm^3, the extrafiber porosity is

$$\varepsilon_o = 1 - \alpha c \tag{5}$$

which can be used instead of ε in Equation 4, with the assumption that $\kappa = 5.55$, to yield

$$K = \frac{1}{5.55 S_o^2} \frac{(1-\alpha c)^3}{\alpha^2 c^2}. \tag{6}$$

Now we note that $\alpha S_o = S$, where S is the flow-exposed surface area of the fibers per unit mass, commonly called the specific surface area. Incorporating this definition into Equation 6 and rearranging, we obtain

$$(Kc^2)^{1/3} = \left(\frac{1}{5.55\ S^2}\right)^{1/3} (1-\alpha c) \tag{7}$$

which is a classic equation that has been applied frequently to pulp mats (9). By plotting permeability data from a single sample at various compressive loads as $(Kc^2)^{1/3}$ versus c, the specific volume, α, can be obtained from the slope and the specific surface, S, can be obtained from the intercept. For example, typical values for lightly refined kraft pulps may be $S = 2\ m^2/g$ and $\alpha = 1.44\ cm^3/g$.

If we assume $\varepsilon_{rel} = \varepsilon_o$, then α can be used with Equation 5 above to give

$$\varepsilon_{rel} \approx \frac{\varepsilon_o}{\varepsilon} = \frac{1-\alpha c}{\varepsilon} = \frac{1-\alpha \rho_s (1-\varepsilon)}{\varepsilon}. \tag{8}$$

Figure 2 below shows ε_{rel} as a function of ε for several typical values of specific volume (based on IPST measurements for many pulp types). As with WRR, α will decrease with compression.

These formulae give relative porosity values, $\varepsilon_{eff}/\varepsilon$, much less than unity. For example, a fibrous web with a porosity of 50% would have $\varepsilon_{rel} = 0.174$. Figure 4 shows predicted relative porosity as a function of total porosity.

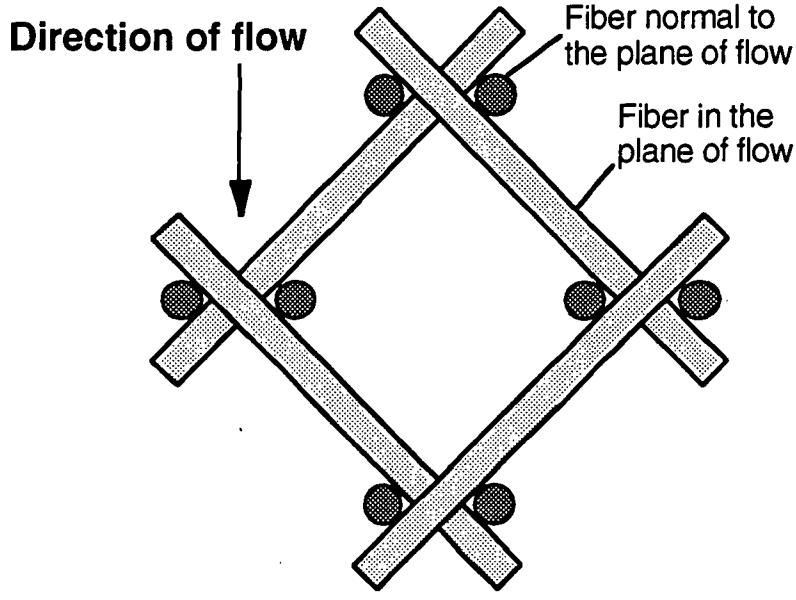

Figure 3. Unit cell of a fibrous medium used in the analysis of Kyan et al. (10).

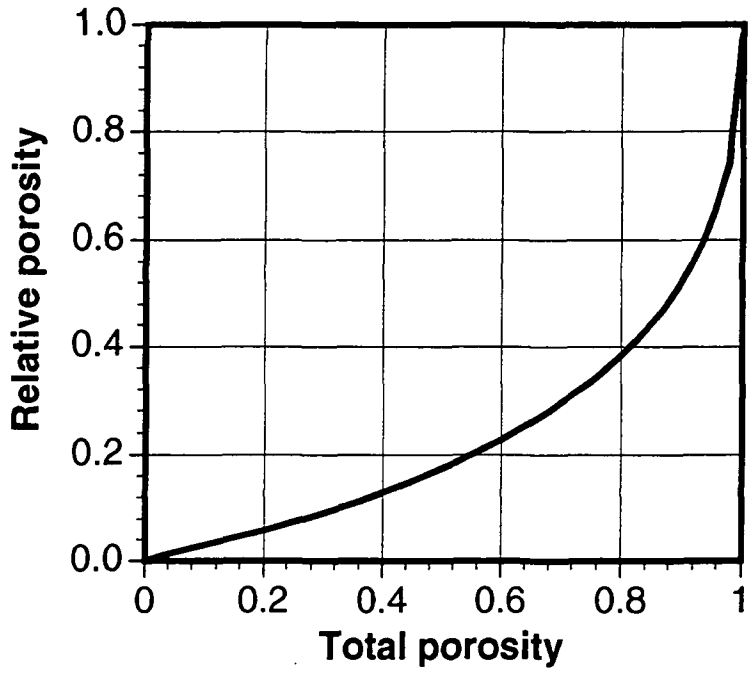

Figure 4. Predicted relative porosity based on the approach of Kyan et al. (10).

In the case of a swollen fiber, the porosity used in Equations 9 and 10 should be the extrafiber porosity, ε_0, if we assume that water trapped in the fiber does not flow. Again, we can use WRR or specific volume data to estimate ε_0 as a function of ε, and then obtain new estimates for relative porosity based on Kyan's approach. The results are shown in Figure 5 for several values of specific volume, including the specific volume for completely unhydrated cellulose, 0.65 cc/g.

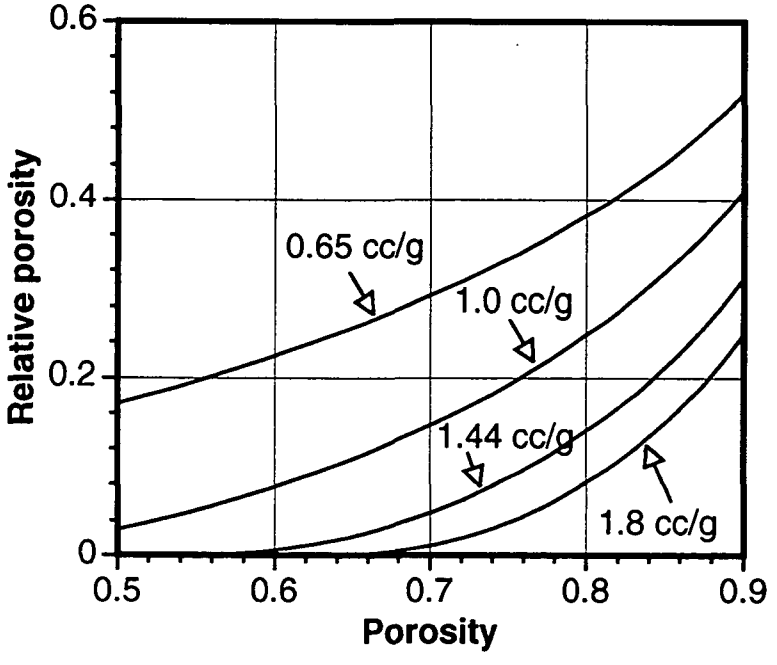

Figure 5. Relative porosity results based on a combination of Kyan's model (10) and extrafiber porosity analysis. Unhydrated fiber corresponds to α = 0.65 cc/g.

Significant reductions in relative porosity are predicted with swelling. In general, in the total porosity range of 0.6 to 0.75, where we expect typical furnishes to have specific volumes of roughly 1.0 cc/g or higher, the predicted relative porosity should be no more than 20%, based on our application of the only known model for relative porosity in a fibrous medium. In that same total porosity range, however, relative porosities as high as 80% could be achieved if the extrafiber pore space were free of dead-end pores and other zones of stagnant fluid. We will now test the applicability of the above analyses with experimental methods.

EXPERIMENTAL APPROACH

Here, we extend experimental methods for in-plane fluid flow measurements that were developed at the Institute of Paper Science and Technology (11-14) and at TRI (15-18). The concept we employ is in-plane radial injection of a colored fluid into the center of a disk of paper. The paper is restrained between two smooth, uniformly pressed platens, which seal the surfaces of the sheet and allow flow to occur only in the radial direction. As the dye spreads into the sheet, it flows through pores open to flow. By comparing the volume occupied by the injected dye in the sheet with the volume of dye actually injected, we can determine the relative porosity (details of the calculation are given below). This can be done for both saturated sheets and initially dry sheets, although dry sheets pose the risk of air bubbles hindering fluid penetration and decreasing the measured relative porosity.

Our apparatus is a modification of the IPST lateral permeability device, which has been previously described (19). In order to observe the growth of a dyed region during in-plane fluid injection, we replaced a metal platen in the permeability apparatus with a device to allow optical access to the compressed sheet. The platen replacement is a large cube of transparent, rigid plastic which will transmit force from the Carver press assembly to the paper (see Figure 6). A metallic mirror oriented at 45° from horizontal was cast into a plastic cube, as shown in Figure 7. The use of a mirror to observe in-plane fluid flow was inspired by the work of Adams et al. (15-17) at TRI. The mirror allows a viewer or a camera standing in front of the cube to observe the paper while it is under compression between the plastic cube and the lower platen. The growth of a dyed zone, formed by injection of colored water through the lower platen, can be viewed during a run. Normally, only the final boundary of the dyed region is noted after a given volume of fluid has been injected.

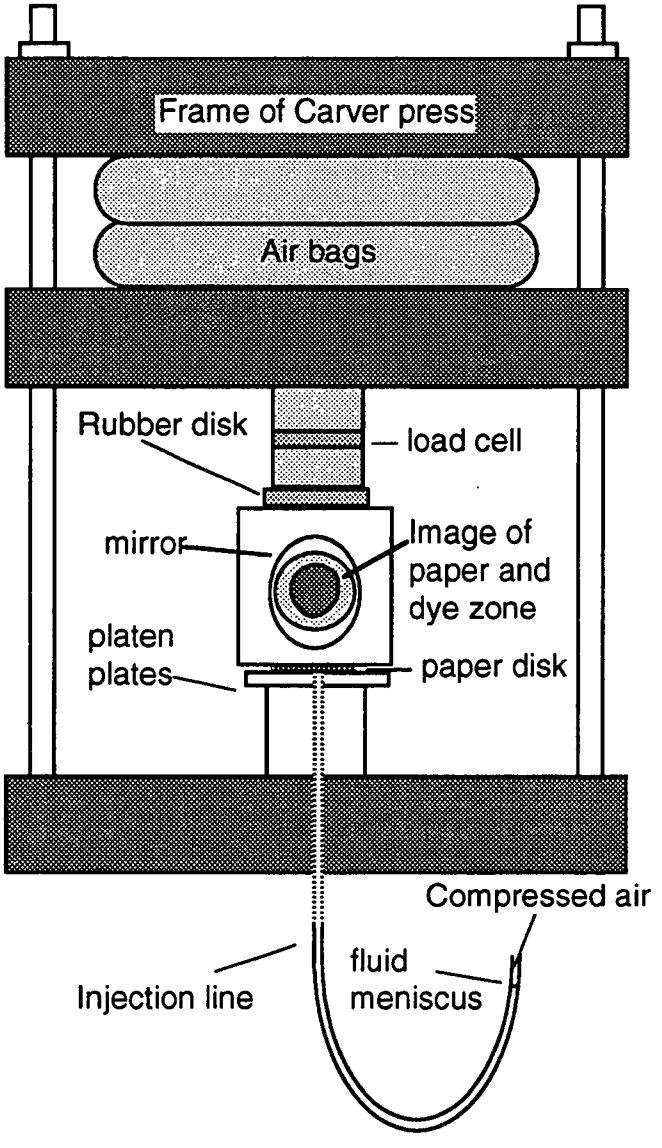

Figure 6. Modified lateral flow apparatus for dye injection tests.

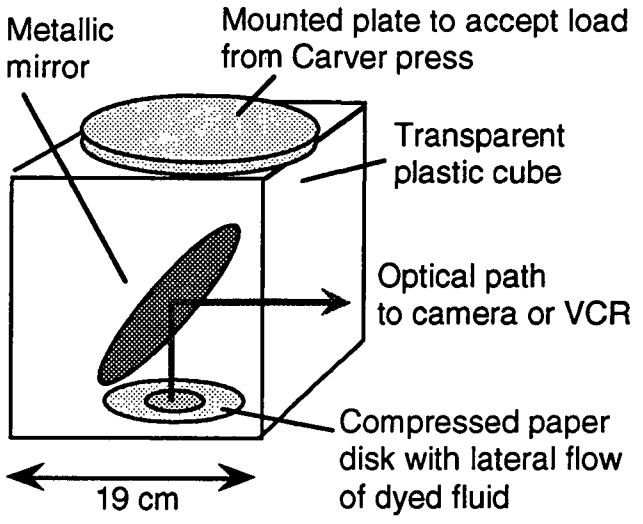

Figure 7. Plastic pressing block with mirror for optical access to a compressed sheet.

The idea of our method is simple: inject fluid into paper, and compare the volume of fluid injected to the volume of the dyed region (based on thickness and dyed area) multiplied by sheet porosity. Sheet porosity is determined from sheet thickness under compression and basis weight:

$$\varepsilon = 1 - \frac{BW}{\rho_c L}, \tag{11}$$

where BW is the sheet basis weight, ρ_c is the matrix density (e.g., the density of pure cellulose in filler-free sheets), and L is the sheet thickness. The area of the dyed zone can be measured after injection, or if the sheet has been marked with measured lines, the dyed area can be determined at various intervals during dye injection by viewing the dye boundary through the plastic cube.

Thickness is determined from three LVDT sensors distributed around the lower platen. LVDT rods protrude from the lower surface of the plastic block. The signal from the sensors responds monotonically to the position of the rods in the sensor. The thickness readings from the three sensors are averaged to give the sheet thickness.

In sheets that were initially dry, saturation was performed under vacuum to reduce the presence of air bubbles in the sheet. We placed a dry sample on a support stand in a desiccator jar containing a layer of water at the bottom. The lid was placed on the jar and vacuum applied to deaerate the sheet. The jar was then

This process will dilute the dye, but should have little effect on the observed motion of the dye boundary. Diffusion of dye in the flow direction may also occur, but generally will be much slower than the flow and can be neglected.

More importantly, dispersion of the dye in the flow direction will occur, inflating the size of the dyed boundary and deflating our estimates of relative porosity. Dispersion is a convective mixing process that arises because of velocity profiles in individual pores and because of the complex branching and intertwining of flow paths in a porous medium. In problems of miscible displacement in porous media, dispersion effects will blur an initially sharp concentration gradient as it advances. Dispersion in the flow direction (radially outward) will inflate the apparent growth of the dyed region (thus deflating our estimate of effective porosity).

Following the Results section of this paper, we explore several aspects of dispersion with analytical and numerical solutions to the relevant but simplified flow problems. We will see that molecular diffusion reduces the degree of dispersion. While dispersion does introduce some error into our results, we will show that it need not be serious if the molecular diffusions of the dye are sufficiently large or if the initial dye concentration is properly adjusted. In any case, dispersion will tend to decrease the measured relative porosity, so our reported values may generally be taken as lower bounds.

Another issue to consider is the z-direction uniformity of the dye. Initial nonuniformities may occur (e.g., if dye flows preferentially along the bottom side of the sheet) which require time for z-direction diffusion and dispersion to even out. We have found that a dyed zoned diameter over 5 cm gives good results in terms of z-direction uniformity of the dyed boundary. If we determine relative porosity using smaller zones, two-sidedness in the dyed zone may inflate the estimate of relative porosity. In highly permeable samples, such as ceramic paper, good uniformity also requires higher injection rates.

As the boundary exceeds about 10 cm, a significant decrease in relative porosity may occur due to dispersion, depending on the pore structure. In making measurements, we generally inject enough dye to obtain a dye boundary between 5 and 10 cm. Below we will report observed changes in relative porosity with the size of the dyed zone.

RESULTS

We have measured relative porosity in a variety of papers, including hardwood and softwood, bleached and unbleached pulp, virgin and recycled furnishes, some newsprint samples, handsheets and commercially made papers, initially saturated and initially dry sheets, and several samples of ceramic paper (made on a paper machine using ceramic fibers). In general, we have found relative porosity to exceed 40%, with values much higher than those predicted by the equation of Kyan et al. (10). In terms of the extrafiber porosity, based on hydrodynamic specific volume, we estimate that roughly 90% of the extrafiber porosity is open to flow. Specific examples are now presented.

Bleached Kraft Handsheets

Several of the earliest measurements in this study were with handsheets from a bleached kraft southern softwood furnish with a freeness of 700 ml CSF. Results for several replicate tests are shown in Table 2. Good reproducibility was achieved. (The diameter of the dyed zone in these samples ranged from 4.7 to 5.6 cm.) At 81% total porosity, the geometric model of Kyan predicts that completely unhydrated fibers would have a relative porosity of 40%. Achieving a relative porosity of at least 45% (assuming our values are lower estimates) for a hydrated pulp (specific volume estimated at 1.2 g/cm^3) implies that the model of Kyan et al. (10) significantly underpredicts relative porosity for paper and possibly other fibrous materials.

Total porosity	Relative porosity
0.814	0.471
0.817	0.454
0.815	0.446
0.817	0.465
0.812	0.458
AVG:	**0.459**

Table 2. Replicate relative porosity values for tests with handsheets of never-dried bleached southern softwood kraft pulp.

Following three months of storage in a cold room, two additional handsheets of the bleached kraft softwood pulp were tested. Blue dextran 2000 was used as the dye. Similar results were obtained, as shown in Table 3.

Total porosity	Relative porosity
0.825	0.535
0.766	0.396

Table 3. Replicate relative porosity values for tests with handsheets of never-dried bleached southern softwood kraft pulp.

Subsequent tests were conducted in additional sheets to determine the effect of dye zone size on apparent relative porosity. Results for several sheets are shown in Figure 9. These sheets all had compressed total porosities in the range of 0.77 to 0.82. The effect of dye diameter appears strong for these samples. While dispersion can reduce the measured relative porosity as the dye diameter grows, an estimate of 40-50% for relative porosity is reasonable in this case. The true relative porosity could be higher.

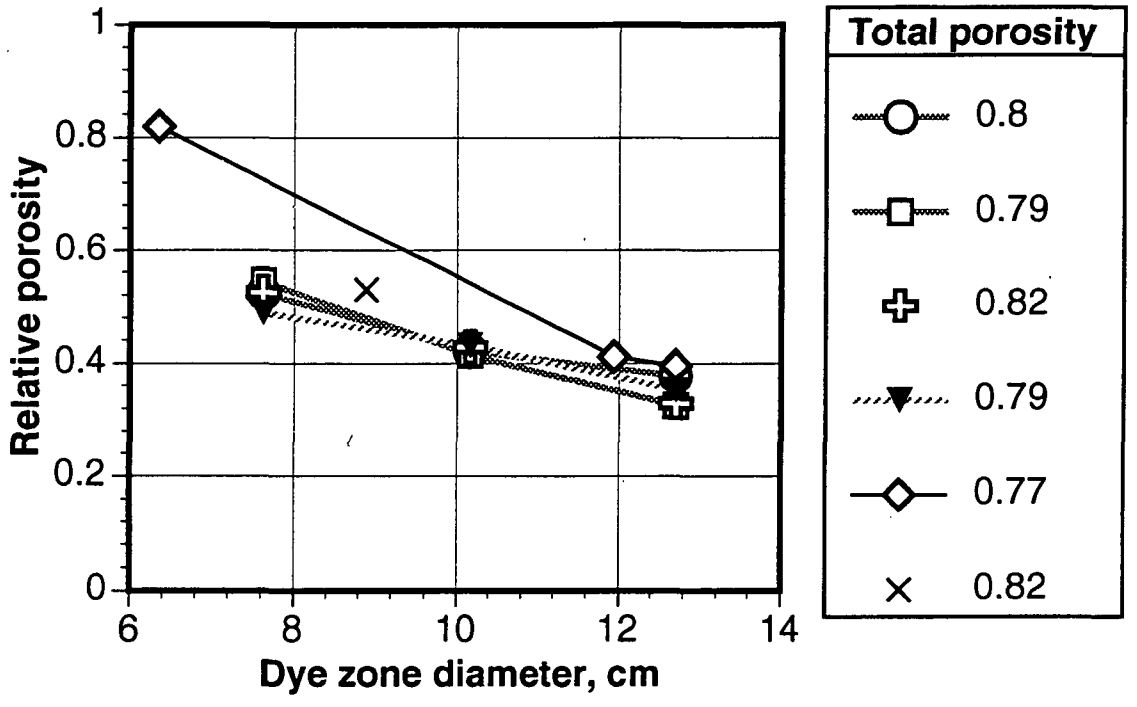

Figure 9. Relative porosity versus dye diameter in bleached kraft handsheets.

Unbleached Kraft Sheets

We also obtained useful results with an unbleached kraft furnish made from southern softwood (a commercial linerboard bottom sheet furnish). Relative porosity data were obtained for 200-gsm sheets. The pulp was never-dried. In one set of tests (Series A), we injected a quantity of dye into the sheets and then

measured the size of dye zone after the sample was removed from the test apparatus. The dye zone diameters fell into the usual range of 6-10 cm. In Series B, we injected dye until it reached the boundary of the paper. We wished to track the dye motion in the sheet, but viewing the dark dye in the dark paper under compression was difficult. However, through the plastic cube we could easily see when dye began leaving the edge of the sheet. We varied load to obtain a small range of porosity values.

We also made measurements in a sheet made from the same furnish after recycling; i.e., handsheets made from the never-dried pulp were dried in a 105°C oven, then slurried and formed into a new 200-gsm handsheet. We compare the never-dried, virgin fiber handsheets with the recycled sheets in Figure 10. Also shown are results for a commercial OCC furnish from the same mill that produced the virgin linerboard furnish. The OCC and the recycled fibers have a higher relative porosity at a given true porosity than the never-dried pulp. Fibers that have been dried are expected to have a lower specific volume, resulting in relatively more interfiber pore space open to flow.

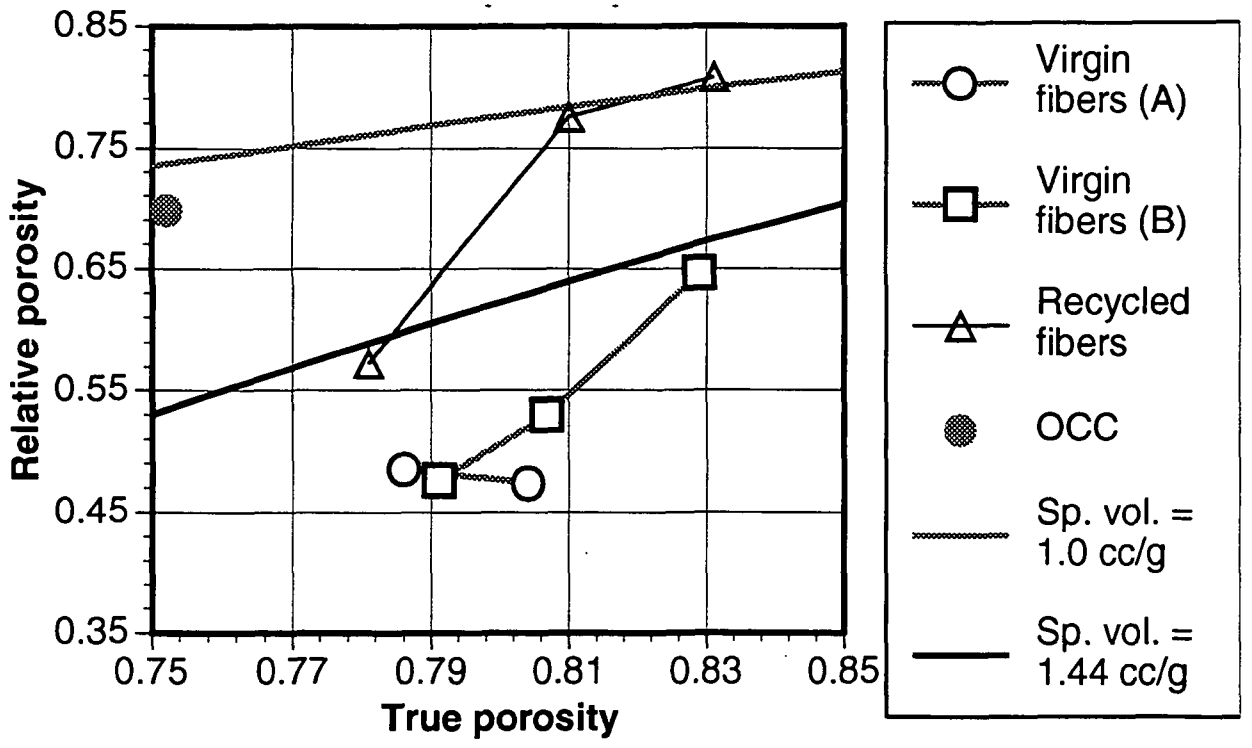

Figure 10. Relative porosity in virgin and recycled unbleached kraft sheets. Extrafiber pore space curves are also shown (see Figure 2).

We used the IPST permeability device (19) to measure the z-direction permeability to water of sheets made from virgin and recycled fibers. Measurements in five 200-gsm sheets of virgin fiber gave specific volume values between 1.39 and 1.55 cc/g. Measurements in three recycled sheets (made from dried and reslurried virgin fiber) gave specific volumes between 1.14 and 1.21 cc/g. The extrafiber porosity curves from Figure 2 for specific volumes of 1.0 cc/g and 1.44 cc/g are shown in Figure 10 for comparison. Specific volume data are difficult to obtain with accuracy for swollen fibers, and are based on a variety of empiricisms and inaccurate assumptions, making hydrodynamic specific volume only a rough estimate of the physical state of the compressed fibrous medium. However, if most or all of the extrafiber pore space is available to flow, we can say that our measurements of relative porosity in the virgin and recycled unbleached kraft sheets are roughly consistent with our estimates of extrafiber pore space derived from permeability measurements. Flow access to most of the extrafiber pore space strongly contradicts the geometrical model of Kyan et al. (10).

Much of the work with unbleached furnishes was conducted before we completed our analysis of dispersion, which is presented below. In these tests, we did not notice a significant dependence of relative porosity on dye zone diameter; i.e., similar results were obtained in virgin sheets for dye zones from 6 to 12.7 cm in diameter. In retrospect, the difficulty of detecting diluted dye in a dark sheet probably prevented dispersion from affecting our results significantly, as we will discuss below.

Other Papers

For a variety of other paper samples, we have consistently found relative porosity values above 40% for the total porosity range of 0.65 to 0.8. Recent work with sheets made from bleached hardwood pulps and with ONP pulp have confirmed this. Sample results for some commercial blotter paper samples are now presented. After vacuum deaeration and water infiltration, wet blotter paper disks (ca. 240 gsm) were particularly easy to work with.

Relative porosity results for wet blotter paper as a function of dye zone diameter are shown in Figure 11. Results for four samples are shown, listed by the total porosity that existed during the measurement (all around 70% total porosity). Since blotter paper has directionality, with a machine direction permeability around 10-30% greater than the cross-direction permeability (11), the injected dye zone tends to be elliptical. When the dye zone was clearly elliptical as opposed to circular, the diameter we report is the average of the major and minor axes. In

Figure 11, we see that the smallest diameters lead to the greatest effective porosity values. In these samples, we suspect that diameters of 5 cm and less are subject to errors due to z-direction nonuniformity of the dye, as discussed above. Our standard procedures call for taking measurements in the range of 7-10 cm, with higher diameters sometimes necessary. There is still considerable variability with diameter in this range, but we can bracket relative porosity within the range of 60-90% for these sheets. Using a specific volume of 1.0 cc/g for blotter paper, the available extrafiber porosity is around 75% for these sheets, which is in the middle of our range for relative porosity. It appears that very little of the extrafiber pore space is taken up by dead-end pores.

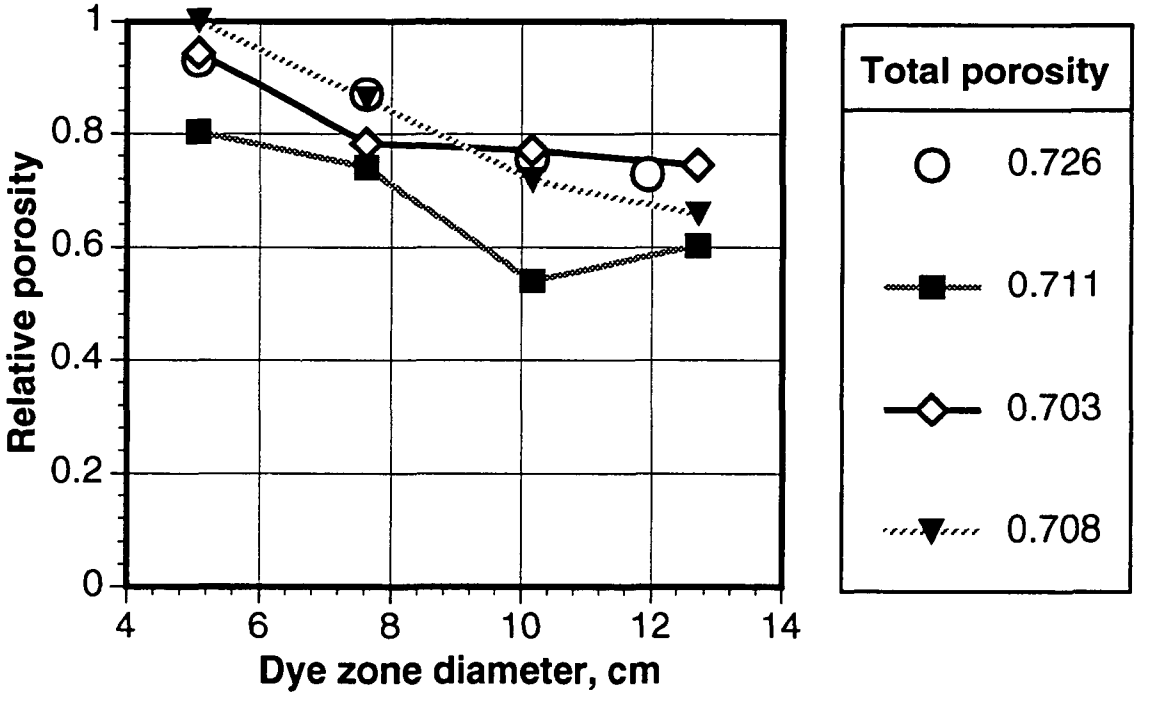

Figure 11. Relative porosity results in saturated blotter paper as a function of dye zone diameter injected into the sheet.

We have also tested samples of ceramic paper produced by Thermal Ceramics (Augusta, Georgia) as a filter material for automotive airbags. The paper is formed on a pilot paper machine from cylindrical alumina and silica fibers. The basis weight of these samples is 725 g/m^2. These samples were vacuum deaerated and soaked with water. The samples were two-sided, leading to some problems in obtaining uniform dye flow in the z-direction, especially when injecting dye into dry samples. Measurements in three vacuum-deaerated and saturated samples gave relative porosities ranging from 79% to 99%. Repeat runs with one sample gave 79% relative porosity for a 9-cm dyed zone in one run, and 83% for a 12.7-cm

dyed zone in a subsequent run (the sample was resaturated for the second run). In these runs, the porosity was between 80 and 81%. In another sample compressed to a porosity of 73%, the relative porosity value we measured was 88%. In a single run with a third sample, dye injected to 9 cm gave 88% porosity, and at 12.7 cm we calculated 99% relative porosity. The latter measurement may have been hampered by two-sidedness problems that made the visible dye region larger than the dye zone lower in the sheet. A value of 80-90% for relative porosity in these samples is about three times higher than Kyan's model would suggest.

Initially Dry Samples

We conducted a variety of tests featuring dye injection into dry blotter paper and dry ceramic paper. Such tests are of limited value, for capillary forces and chemical and physical absorption will pull water into pores that are not really open to flow. However, the "two-phase relative porosity" results will be an indication of the pore space that does not remain occupied by air bubbles after forced infiltration of water. The pore space occupied by air bubbles that could not be displaced by liquid provides some information about the pore structure.

Table 4 shows "dry relative porosity" values for three series of tests with 240 g/m^2 blotter paper. (A subsequent measurement using blue dextran 2000 as the dye gave a relative porosity of 0.79 in a sheet at a porosity of 0.68.) These results were obtained by several operators using slightly different procedures. In spite of the scatter in the data, the amount of trapped air in the sheet appeared to be low, suggesting that there are few large voids which cannot be accessed by water as it flows and diffuses into the open structure of these papers.

Series I		**Series II**		**Series III**	
ε	Dry ε_{rel}	ε	Dry ε_{rel}	ε	Dry ε_{rel}
0.771	0.936	0.778	0.583	0.649	0.699
0.773	0.836	0.777	0.712	0.647	0.854
0.769	0.974	0.782	0.747	0.656	0.891
0.771	1.004	0.777	0.668	0.648	0.801
0.772	0.933	0.778	0.803	0.649	0.962
0.768	0.810				
AVG:	**0.916**	**AVG**	**0.703**	**AVG**	**0.841**

Table 4. Dry (apparent) relative porosity from injection into dry blotter paper sheets.

The case of water infiltration into a dry sheet involves many complications, including time-dependent swelling, surface diffusion, capillary flows, and relative permeability. However, measurements of dry relative porosity could provide useful information to assist in better understanding such flows in the future. Future work is planned using injection of nonswelling fluids to avoid water uptake into pores that would normally be unavailable to flow.

DISPERSION ANALYSIS

Here we will consider some of the transport phenomena that complicate our simple approach. Readers not desiring a more fundamental understanding of the associated flow issues in our study may wish to advance to the Discussion section.

The issue of dispersion will be considered in two simple ways. We will first consider the dispersion that occurs at a microscopic level in a single cylindrical pore extending through a porous medium. Then we will treat the averaged, macroscopic case of dispersion in a porous medium using a radial geometry that corresponds to our experimental conditions. In both cases we will consider how the dispersion of an initially sharp dye boundary may affect our relative porosity results.

Dispersion in a Capillary Tube: The Taylor Dispersion Problem

Flow in a single pore can be simulated as laminar flow in a cylindrical capillary tube. The parabolic velocity profile for laminar flow leads to dispersion, for the fluid traveling in the middle of the tube flows at twice the average velocity, while the fluid at the walls has zero velocity. If a sharp boundary between dyed fluid and clear fluid existed initially, this boundary will soon be spread out in the flow direction, as depicted in Figure 12.

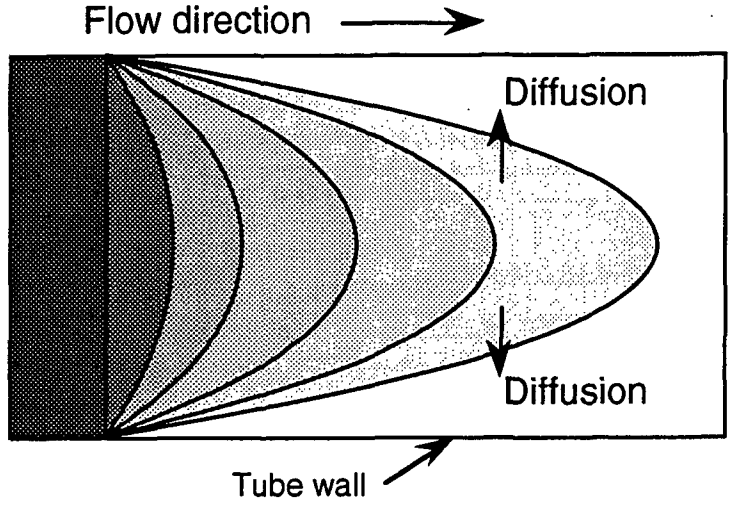

Figure 12. Distortion of a flat dye-water boundary moving in a flow with a parabolic velocity profile. Some of the dye advances faster than the average flow velocity.

The dispersion of the dye boundary is partially countered as dye from the fast-flowing center of the tube diffuses into slower moving fluid. If diffusion is rapid, the advancing dye front becomes narrow (assuming that the axial flow is fast compared to axial diffusion).

The simplified convection equation for this problem is

$$\frac{\partial C}{\partial t} = D_d\left(\frac{\partial^2 C}{\partial r^2} + \frac{1}{r}\frac{\partial C}{\partial r} + \frac{\partial^2 C}{\partial x^2}\right) - 2\overline{V}\left(1 - \frac{r^2}{R^2}\right)\frac{\partial C}{\partial x} \qquad (12)$$

where C is the concentration of dye, t is time, r is the radial distance from the centerline of the capillary, R is the radius of the capillary, x is distance in the flow direction, and $\overline{V}$ is the average velocity of the fluid. In Equation 12, dye transport in the x-direction is assumed to occur predominantly by axial convection rather than molecular diffusion, so the term for diffusion in the x-direction has been dropped. Taylor (20,21) has provided approximate solutions for this problem, depending on the flow characteristics. If

$$\frac{2L}{\overline{V}} >> \frac{R^2}{14D_d}, \qquad (13)$$

where L is the distance downstream from the original dye front, then radial diffusion dominates. In that case, at a distance x downstream from the original dye boundary, the ratio of average dye concentration, C_{avg}, to the undispersed (initial) dye concentration, C_o, is:

$$\frac{C_{avg}}{C_o} = \frac{1}{2}\left(1 \pm \text{erf}\frac{x - Vt}{2\sqrt{D't}}\right) \tag{14}$$

where D' is a dispersion coefficient related to the average velocity and the molecular diffusion coefficient, D_d, by

$$D' = \frac{R^2 \overline{V}^2}{48 D_d}. \tag{15}$$

The length of the transition zone, defined as the region in which concentration varies from 10% to 90% of C_o, is given by

$$L_{tr} = 0.52 R \overline{V} \sqrt{\frac{t}{D_d}} \tag{16}$$

which shows that the rapid diffusion leads to a plug flow motion of the displacing fluid, in spite of the parabolic velocity profile (22).

The Versatint Purple II dye is a proprietary polymer-based dye with a molecular weight near 9000. Although diffusion coefficients are not available for this dye, the value for diffusion in water probably lies in the range of 1×10^{-7} to 1×10^{-6} cm^2/s, based on reported coefficients for other polymers of similar molecular weight (23). Using the limits of this range, we can calculate the dispersion in the dye front. In Figure 13, we show the results for a true dye-injection distance of 5 cm ($t^* \overline{V}$ =5 cm) through a 100 μm pore with a mean velocity of 0.05 cm/s (a representative velocity for much of our work). Axial convection in the tube makes some dye present well beyond the "correct" penetration distance of 5 cm. If a dye with D_d = 1×10^{-7} cm/s were used, and if a concentration only 10% of the original dye concentration would be identified as the edge of the dye boundary, then the experimenter would report 5.4 cm as the distance of dye penetration instead of 5.0 cm, and the estimated relative porosity would be underestimated by about 10%. The assumed pore size of 100 μm is larger than most pores in paper; smaller pore sizes lead to decreased dispersion, so the estimate of 10% error may be an upper limit for this line of analysis. Of course, this analysis is based on flow in a single tube, which overlooks the real nature of the dispersion problem in a complex porous medium. A more appropriate approach is now considered.

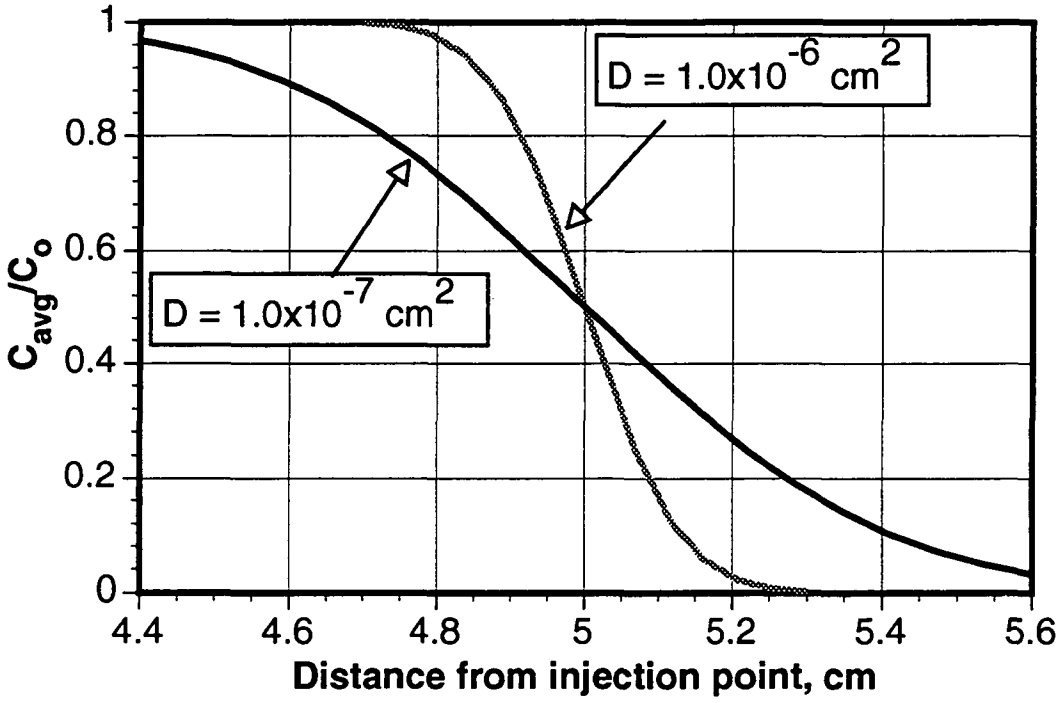

Figure 13. Predicted dispersion of a dye boundary after 5 cm travel in a capillary tube.

Dispersion in a Porous Medium

A real porous medium has a complex network of pores and throats which is best treated at the macroscopic level using empirical parameters such as permeability to describe the average transport behavior of the system. The geometry we will deal with is shown in Figure 14. We will treat the porous medium as a homogeneous continuum, with a steady, radially symmetric velocity field emanating from the injection port. At time t = 0, the injected water is replaced with a slug of aqueous dye solution having the same properties as water except for the dye concentration. Our fundamental transport equation (averaged over the homogenous porous medium) becomes

$$\frac{\partial C}{\partial t} + v(r)\frac{\partial C}{\partial r} = \frac{1}{r}\frac{\partial}{\partial r}\left(rD\frac{\partial C}{\partial r}\right) \tag{17}$$

where D is the effective dispersion coefficient in the porous medium in m^2/s, and v(r) defines the velocity field as a function of radial position. For steady radial flow in a fibrous mat, with an inlet port of size r_i and a mat diameter of r_o, the velocity is given by

$$v(r) = \frac{K\Delta P}{\mu r \ln(r_o/r_i)} \equiv \frac{B}{r} \tag{18}$$

where ΔP is the difference between the injection pressure and atmospheric pressure, μ is the fluid viscosity, and B is a constant for a given flow condition. geometry, fluid, and pressure drop across the sample. If we combine Equations 17 and 18, and assume that the effective dispersion coefficient is a constant, the dye transport equation becomes

$$\frac{\partial C}{\partial t} = D\left(\frac{\partial^2 C}{\partial r^2} + \frac{1}{r}\frac{\partial C}{\partial r}\right) - \frac{B}{r}\frac{\partial C}{\partial r}. \tag{19}$$

In dimensionless form, this becomes

$$\frac{\partial C'}{\partial \tau} + \frac{(P-1)}{r'}\frac{\partial C'}{\partial r'} = \frac{\partial^2 C'}{\partial r'^2} \tag{20}$$

where $\tau \equiv Dt/\Delta r^2$ ($\Delta r = r_o - r_i$), $r' \equiv r/\Delta r$, $C' \equiv C/C_o$ (C_o is the initial dye concentration), and $P \equiv B/D$ or $rV(r)/D$, which we term the radial Peclet number (as opposed to the "pore" Peclet number, introduced below).

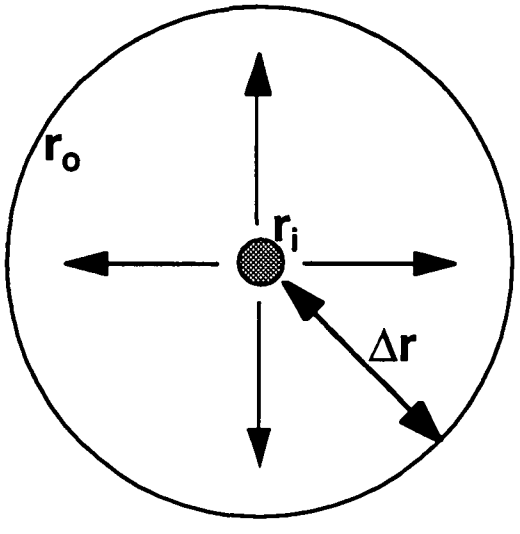

Figure 14. Radial geometry of fibrous mat with dye injection flow.

The assumption of constant dispersion coefficient is helpful in performing a crude analysis of this problem, but in reality the dispersion coefficient will vary with position since it is a function of flow velocity. Greenkorn (24) provides a useful discussion of longitudinal dispersion and its complex relationship to flow velocity and molecular diffusion. The dimensionless dispersion number, D/D_d, is

a function of the pore Peclet number, $Pe \equiv a\overline{V}/D_d$, where a is the average pore radius. For the flows used for this study, pore Peclet numbers greater than 20 are typical, for which we may use the approximate relationship

$$\frac{D}{D_d} \approx \gamma Pe^{1.2} \tag{21}$$

where γ is an empirical parameter on the order of unity. In considering the relationship between P in Equation 20 and the terms in Equations 21 and 18, we see that either a high molecular diffusivity or a low flow velocity increases P, which means that convection of the dye boundary dominates over dispersion of the boundary. One of the mechanisms that reduces the impact of dispersion when molecular diffusion is high or velocity is low is the Taylor dispersion mechanism we considered above (e.g., see Equation 15). However, our analysis has assumed that the velocity is at least high enough to make longitudinal diffusion negligible compared to convection. If the velocity is too low ($Pe < 1$), then dispersion would become high due to longitudinal diffusion.

Application of estimated flow and diffusion parameters for our problems indicates that the radial Peclet number, P, should be no less than 100 and is more likely on the order of 1000. Even though Equation 20 is approximate and does not properly consider the variation of D with position, we will solve it for our problem to gain rough insights into the effect of dispersion on our results. (We have also solved the transport problem using two different forms of a variable dispersion coefficient that includes the effect of velocity variation in the flow field. The effect of variation in the dispersion coefficient for our problem proves to be minor. The numerical results thus obtained do not differ in substance from those reported here.)

The initial condition and boundary conditions are:

$$\tau = 0: \; C' = 0$$

$$r' = r_i/\Delta r: \; C'=1 \; (\tau>0)$$

$$r' = r_o/\Delta r: \; \partial C'/\partial r' = 0.$$

We used a finite difference approach (explicit form with second-order central differencing and upwind differencing of convective terms) to solve Equation 20 for various values of P. Results are shown in Figures 15 through 17 for P values of 10, 100, and 1000. In each of these figures, we show four different breakthrough curves corresponding to dye breakthrough at locations of $\Delta r/4$, $\Delta r/2$, $3\Delta r/4$, and Δr

(Δr is the distance from the edge of the injection port to the edge of the paper disk, or 6.35 cm - 0.28 cm = 6.07 cm). Breakthrough is arbitrarily defined as the moment when dye at a concentration of $0.1C_o$ first appears at the location of interest. The breakthrough points are marked in each figure.

In Figure 15, P is low enough that dispersion dominates. The dye boundaries are broad and diffuse. Large errors in measurement (ca. 50% or more in calculated relative porosity) could arise if dye at a concentration of $0.1C_o$ was taken as the dye injection boundary. In Figure 16, where P = 100, the effect of convection is more important, and the dye boundary advances with less broadening.

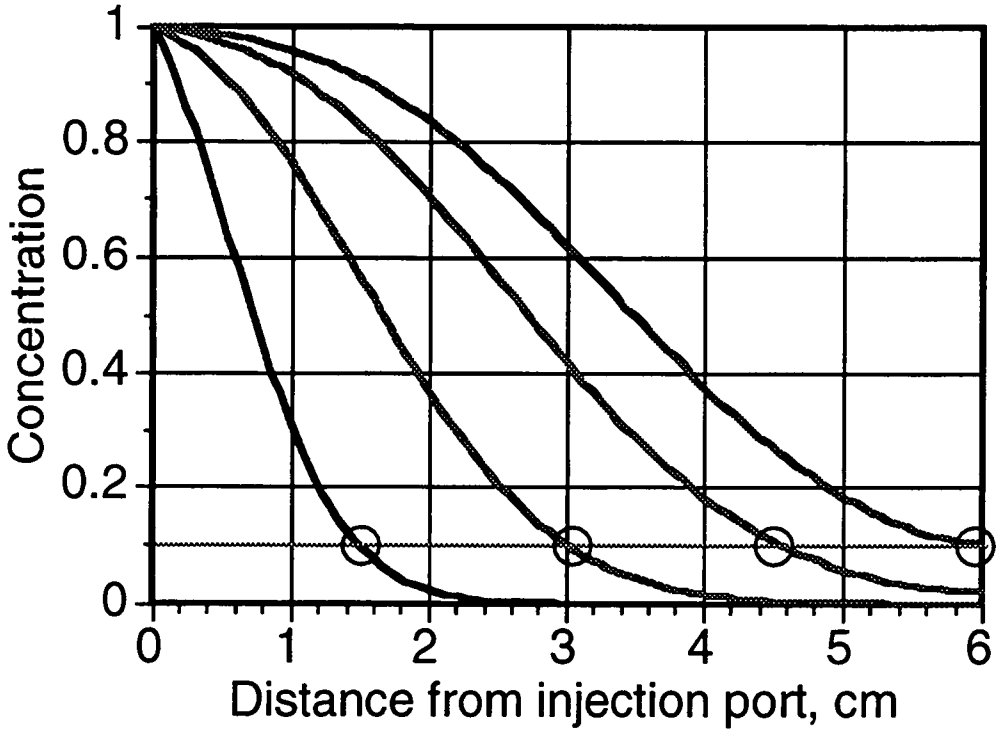

Figure 15. Computed breakthrough curves for P = 10.

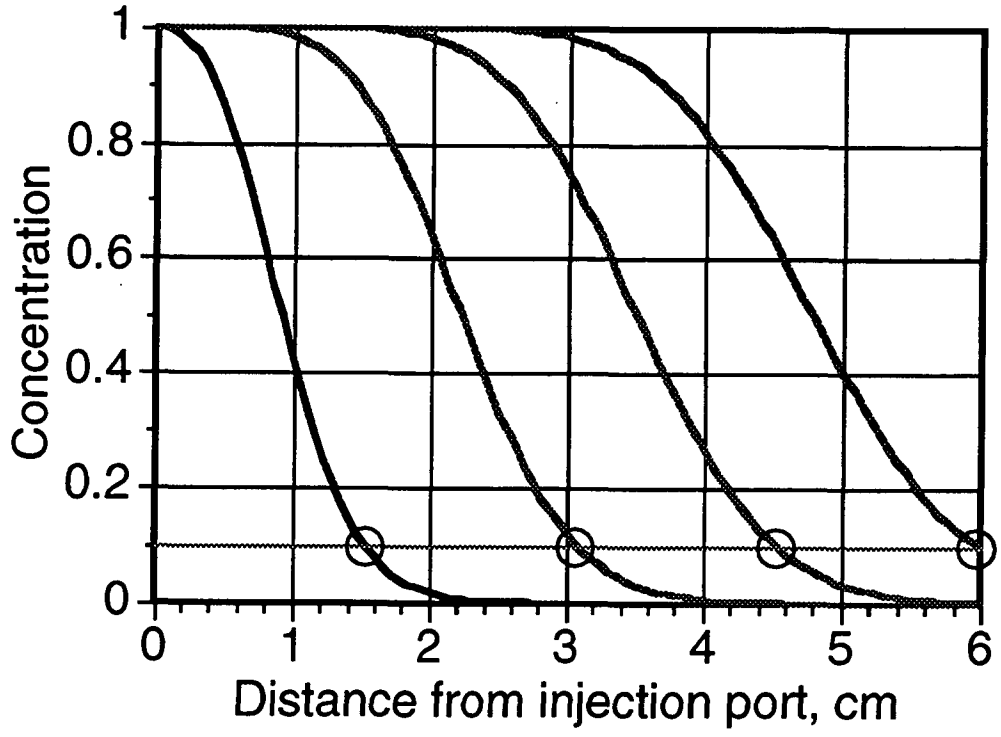

Figure 16. Computed breakthrough curves for P = 100.

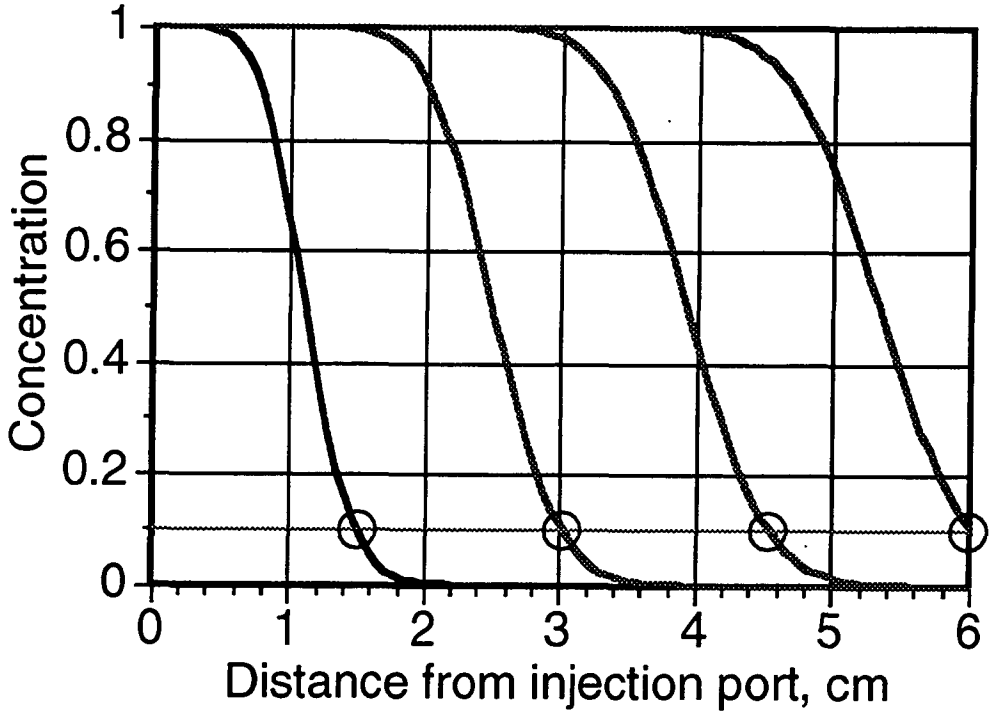

Figure 17. Computed breakthrough curves for P = 1000.

In Figure 17, where the P value of 1000 is more representative of our experimental conditions, dye concentration boundaries are narrower still. For example, consider an experiment in which we inject dye until a dye radius of 4.5 cm is detected (4.5 cm corresponds to $3\Delta r/4$, the detection point for third breakthrough curve). A numerical integration of the dye concentration given by the third breakthrough curve shows that the "correct" location of the dye boundary is 3.95 cm from the injection port – in other words, if the same amount of dye were injected with zero dispersion and pure plug flow, the dye boundary would be 3.95 cm. If dye diluted to 10% of the original concentration was mistaken for the "true" dye boundary (which might have been possible in several of our experiments), then we would have used a value of 4.5 cm instead of 3.95 cm for the extent of dye boundary growth. This gives an error of about 25% in the size of the dye boundary, which in turn would deflate the estimated relative porosity by about 20% of its correct value. The "correct" dye concentration to track is about 45% of the injected value (the radial geometry requires this to be less than 50%), which means that if we took a 45% dye solution as the location of the dye boundary, then dispersion would have a negligible effect on our determination of relative porosity. Based on our experimental procedures, we estimate that relative porosity error due to dispersion is usually in the range of 0 to -20%, although we showed some more extreme evidence of dispersion in Figures 9 and 11 above. In many experiments, the dye boundary appeared to be reasonably sharp, with an apparent width less than roughly 0.5 cm. In cases where the dye boundary was not sharp (based on appearance), the boundary used for calculations was taken as the approximate midpoint of the region with a visible dye concentration gradient, which should reduce some of the error caused by dispersion.

The analytical and numerical analyses show that some error is introduced by dye dispersion, but the effect does not jeopardize conclusions based on our simple methods. In fact, if the dye concentration is such that the detected dye boundary corresponds to slightly less than 50% of the injected dye concentration, then the error may be negligible (as it may have been in the tests with unbleached pulp). Dispersion errors will lower our estimates of relative porosity.

DISCUSSION

We have presented several sets of results from a study of relative porosity in fibrous structures. We conclude that much of the extrafiber pore space is available to flow. Adopting our results with nonswelling ceramic fibers, roughly 90% of that pore space may permit flow – at least under an in-plane pressure gradient.

Relative porosity values in paper were observed ranging from roughly 40% to over 80% in the total porosity range of 65 to 80%. These papers were not heavily refined, and based on permeability measurements in these sheets or in sheets from similar pulps, the compressed specific volume is expected to be between 1.0 and 1.5 cm^3/g. Fibers that have been dried (recycled fibers or resaturated blotter paper) will have lower specific volumes than the original virgin fibers.

If we assume that 90% of the extrafiber porosity is open to flow, or $\varepsilon_{rel} = 0.9\ \varepsilon_o$, then our previous results based on specific volume can be modified to make a more realistic prediction of relative porosity. The results are shown in Figure 18. Relative porosity values for moist paper made from lightly refined pulp may typically lie between or near the curves shown.

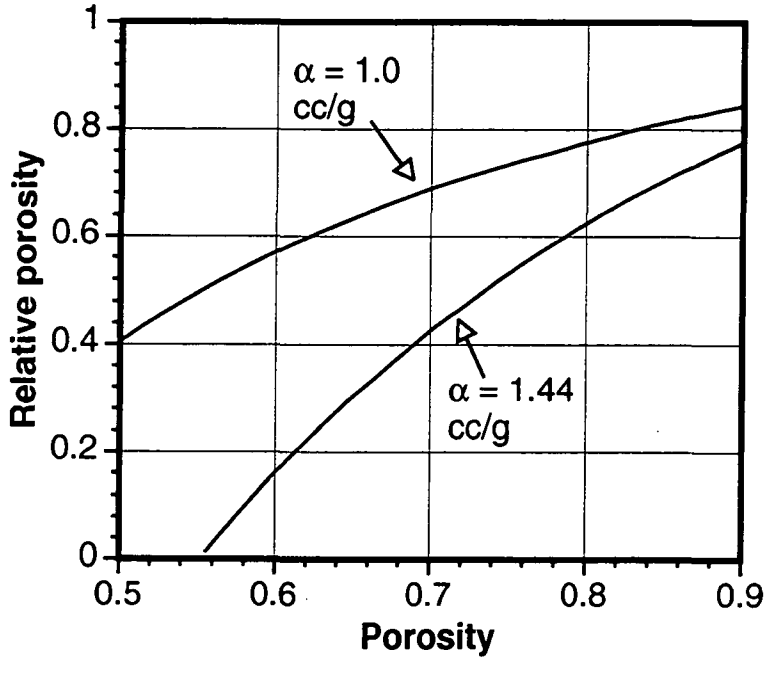

Figure 18. Predicted relative porosity results based on 90% of extrafiber pore space being open to flow. (Compare to Figure 2).

We have only considered relative porosity for in-plane flow. For flow in the transverse direction, it is possible that the differing pore structure could affect relative porosity. For example, flow normal to a flat fiber may have a stagnant zone on the downstream side of the fiber at sufficiently high particle Reynolds numbers (when inertial effects are important). In creeping flow, however, flow over a flattened fiber ought to be able to curve around the fiber surface, leaving no stagnant zones due solely to the fiber shape. But if relative porosity is an anisotropic parameter, we would anticipate a lower value for the transverse direction than for lateral flow.

Our results are subject to several sources of error, including dispersion, and can only be taken as estimates. However, most sources of error will tend to lower the calculated relative porosity. The errors are unlikely to reverse our conclusion that dead-end pores in the extrafiber pore space are relatively insignificant, at least for the papers and the flow conditions of our study.

Applications

Mechanical water removal processes rely on flow of water, which must occur in the open pore space. (As compression occurs, water is squeezed from the cell walls into the open pores where it can flow; the specific volume or WRR is simultaneously reduced.) An understanding of relative porosity is relevant to the limitations of mechanical dewatering. In wet pressing, for example, as the sheet is compressed, a limit is reached when the relative porosity goes to zero in a highly compressed sheet.

Relative porosity is especially important in an alternative to wet pressing, displacement dewatering. In displacement dewatering, high densification of the sheet is avoided by using a gas phase to push liquid water out of the pores of a lightly compressed sheet. The objective is to decouple density and dryness, yielding a dewatered sheet with high bulk. This process has been investigated for several years at IPST (25). The effectiveness of the process will be directly related to the effective porosity. If the effective porosity were unity, in theory, one could hope to displace all of the liquid from the sheet (in reality, viscous fingering and capillary effects would lead to some water retention even then). In practice, we can only remove a fraction of the available water. For example, in a sheet pressed to a porosity level of 70% (giving 40% solids when saturated with water), a reasonable relative porosity value of 50% means that no more than 50% of the fluid in the compressed sheet could be displaced. If this much fluid were displaced, the solids level would be raised from 40% (for a saturated sheet) to 57% with no

significant increase in densification. In practice, only about half of the water in open pores is removed by gas displacement. (This is a rough estimate.) However, the relative porosity value, if known, helps put an upper bound on what could be achieved in an ideal process.

For the penetration of ink, size, or coating color into a dry sheet, dry relative porosity tests may be of some value. Based on our tests with lateral flow, air entrapment in the pores does not seem to be a serious problem. Of course, z-direction relative porosity measurements are needed to properly address this issue.

CONCLUSIONS

The Kyan model for relative porosity appears to underpredict relative porosity values in real fibrous structures. Based on our results here, the extrafiber pore space of a paper structure is largely open to flow, with perhaps only 10% of that space truly confined to dead-end pores or stagnant zones. Of course, the details of the sheet formation will determine what fraction is open to flow. We clearly need to expand our base of results to clarify this issue.

The effects of diffusion and dispersion have been considered and treated analytically and numerically, though with substantial simplification. Our analysis suggests that dispersion can introduce error into our results, but for our procedures (using Versatint Purple II dye) and our flow conditions, this error will often be less than 20% and can be made negligible in some cases.

A thorough investigation of relative porosity, or of two-phase flow processes in paper, should consider the possibility of anisotropy and velocity-dependent effects. To date, we have done neither.

Relative porosity measurements in the thickness direction of paper appear to pose serious experimental challenges. Flow rate effects will be explored, but we expect that they will be minor as long as inertial effects can be neglected (i.e., as long as Darcy's law is sufficient to describe the flow). For most papermaking operations after the forming section, inertial effects are minor (even in wet pressing).

Further work will include measurements with nonswelling fluids injected into paper to better understand the difference in pore structure between wet and dry sheets. Additional studies of recycling effects will also be carried out.

ACKNOWLEDGMENT

Thanks to Tom Merchant, Glenn Dunlap, and Ye Xiao-Liang for technical assistance in this study. Thanks to Bernard Miller of TRI for a valuable discussion. This work was supported by the member companies of the Institute of Paper Science and Technology.

LITERATURE CITED

1. Roux, J. C., and Vincent, J. P., "A Proposed Model in the Analysis of Wet Pressing," Tappi J., 74(2): 189 (Feb. 1991).

2. Ellis, E. P., Jr., "Compressibility and Permeability of Never Dried Bleached Softwood Kraft Pulp and Its Application to the Prediction of Wet Press," Ph.D. Thesis, Chem. Eng. Dept., Univ. of Maine, Orono, Maine, 1981.

3. Robertson, A. A., "The Physical Properties of Wet Webs. Part 1. Fibre-Water Association and Wet Web Behaviour," Tappi J., 42(12): 969 (1959).

4. Robertson, A. A., "The Physical Properties of Wet Webs. Part 2. Fibre Properties and Wet Web Behaviour," Svensk Pappers., 66(12): 477 (1963).

5. Stone, J. E., and Scallan, A. M., "The Effect of Component Removal Upon the Porous Structure of the Cell Wall of Wood. Part III. A Comparison Between the Sulphite and Kraft Processes," Pulp and Paper Canada, 69(12): 69/T288 (June 21, 1968).

6. Carlsson, G., Lindström, T., and Scöremark, C., "Expression of Water From Cellulosic Fibres Under Compressive Loading," Fibre-Water Interactions in Paper-making, Transactions of the Symposium at Oxford, Sept. 1977, British Paper and Board Ind. Fed., London, 1977.

7. Fowler, J. L., and Hertel, K. L., "Flow of a Gas Through Porous Media," J. Appl. Physics, 11: 496-502 (1940).

8. Chen, F. J., "The Permeability of Compressed Fiber Mats and the Effects of Surface Area Reduction and Fiber Geometry," Ph.D. Dissertation, The Institute of Paper Chemistry, Appleton, Wisconsin, June 1982.

9. Carroll, M., and Mason, S. G., "The Measurement of Fiber Swelling by the Liquid Permeability Method," Can. J. Tech., 30(12): 321 (1952).

10. Kyan, C. P., Wasan, D. T., and Kintner, R. C., "Flow of Single-Phase Fluids Through Fibrous Beds," Ind. Eng. Chem. Fundam., 9(4): 596 (1970).

11. Lindsay, J. D., "The Anisotropic Permeability of Paper," Tappi J., 73(5): 223 (May 1990).

12. Lindsay, J. D., and Wallin, J. R., "Characterization of In-Plane Flow in Paper," AIChE Forest Products Division Symposium Series (1992).

13. Lindsay, J. D., "The Anisotropic Permeability of Paper: Theory, Measurements, and Analytical Tools," IPC Technical Paper Series #289, The Institute of Paper Chemistry, Appleton, Wisconsin, 1988.

14. Horstmann, D. H.; Lindsay, J. D., and Stratton, R. A., "Using Edge-Flow Tests to Examine the In-Plane Anisotropic Permeability of Paper," Tappi J., 74(4): 241 (1991).

15. Adams, K. L., and Rebenfeld, L., "In-Plane Flow of Fluids in Fabrics: Structure/Flow Characterization," Textile Research J., 57(11): 647 (1987).

16. Adams, K. L.; Miller, B., and Rebenfeld, L., "Forced In-Plane Flow of an Epoxy Resin in Fibrous Networks," Polymer Eng. and Sci., 26(20): 1434 (1986).

17. Adams, K. L.; Russel, W. B., and Rebenfeld, L., "Radial Penetration of a Viscous Liquid into a Planar Anisotropic Porous Medium," Int. J. Multiphase Flow, 14(2): 203 (1988).

18. Miller, B.; Friedman, H. L., and Amundson, R., "In-plane Flow of Liquids into Fibrous Networks," 1991 TAPPI Nonwovens Conference, Marco Island, Florida, May 1991.

19. Lindsay, J. D., and Brady, P. H., "Studies of Anisotropic Permeability With Applications to Water Removal in Fibrous Webs," Part I, Tappi J., 76(9): 119 (1993).

20. Taylor, G. I., *Proc. Roy. Soc. A*, 219: 186-203 (1953).

21. Taylor, G. I., *Proc. Roy. Soc. A*, 223: 446-468 (1954).

22. Bear, J., *Dynamics of Fluids in Porous Media,* American Elsevier Publ. Co., New York, 1972, p. 585.

23. Brandrup, J., and Immergut, E. H., editors, *Polymer Handbook*, 2nd ed., John Wiley and Sons, New York, pages IV-73 and IV-85.

24. Greenkorn, R. A., *Flow Phenomena in Porous Media*, Marcel Dekker, Inc., New York, 1983, pp. 183-220.

25. Lindsay, J. D., "Displacement Dewatering to Maintain Bulk," Paperi ja Puu, 74(3): 232-242 (1992); also presented at the Helsinki Symposium on Alternate Methods of Pulp and Paper Drying, Helsinki, Finland, June 4-7, 1991.